# Light Curve Analysis for a Stellar System

**M. Jélvez**[1]

[1] Facultad de Ciencias, Universidad de Valparaíso, Av. Gran Bretaña 1111 Playa Ancha.

**Abstract.** This report presents a Fourier analysis of photometric data for a stellar system, with the aim of detecting significant periodicities and classifying the type of observed binary system. The dataset consists of 1646 differential magnitude measurements obtained over an interval of approximately 4.32 hours. The analysis revealed two statistically significant independent frequencies: $f_1 = 5.8346 \pm 6.08 \times 10^{-3}\, d^{-1}$ ($P_1 = 0.1713 \pm 1.78 \times 10^{-4}\, d$) with an amplitude of $0.1909 \pm 2.81 \times 10^{-3}$ mag, and $f_2 = 19.7266 \pm 5.59 \times 10^{-4}\, d^{-1}$ ($P_2 = 0.0506 \pm 10^{-5}\, d$) with an amplitude of $1.4589 \pm 2.89 \times 10^{-3}$ mag. The uncertainties, estimated via Monte Carlo resampling, incorporate the individual photometric errors. A multi-frequency model incorporating these fundamental frequencies and their harmonics successfully reproduces the observed light curve, generating residuals consistent with the photometric errors. The short orbital period of 1.21 hours places the system in the ultra-short period (USP) regime, characteristic of compact post-common-envelope binaries. A comparative period-amplitude analysis strongly favors a post-common-envelope binary scenario, where the primary component could be a hot B subdwarf (sdB) or a white dwarf, and the secondary a brown dwarf or a low-mass white dwarf. The secondary signal ($P_1$) could originate from pulsations of the primary component or from a third body in a hierarchical orbit.

## 1. Introduction

This report aims to analyze real photometric data of a binary star using Fourier analysis techniques, in order to detect significant periodicities and, based on them, classify the type of observed stellar system.

The dataset consists of 1646 photometric observations obtained over an interval of approximately 4.32 hours. The measurements are expressed in differential magnitudes, which allows for the removal of systematic effects associated with the atmosphere and instrumentation, leaving only the intrinsic variation of the object. The observation times are recorded in Julian Days (JD). The corresponding light curve, along with the error associated with each measurement, is presented in **Fig.** 1.

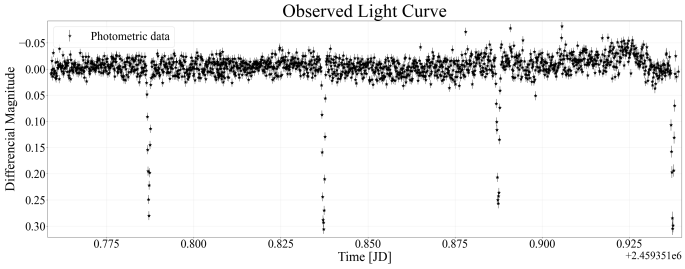


**Fig. 1.** Light curve obtained from 1646 differential photometric measurements recorded over a span of 4.32 hours. Each point represents an individual observation and the vertical bars correspond to the associated measurement error, whose mean value is approximately $7.9{\times}10^{-3}$ mag. A moderate scatter around the mean magnitude is observed, on which we aim to identify periodic variations of astrophysical origin.

These observations constitute the basis for the search of periodicities in the photometric signal. From the frequency analysis, the goal is to determine which peaks detected in the power spectrum correspond to real variations of the source and which could be attributable to noise. For this purpose, the signal-to-noise ratio (SNR) is used as a validation criterion for significant frequencies.
Once the reliable periodicities and their associated parameters have been determined, we proceed to interpret the results physically in order to classify the studied binary system, considering both the obtained period and the morphology of the light curve.

## 2. Methodology

The analysis of photometric variability was based on the application of Fourier transforms to the time series of differential magnitudes obtained for the stellar system. This type of analysis allows for the transition from the time domain to the frequency domain, which facilitates the detection of periodicities present in the photometric signal. To carry out this procedure, the software Period04 (Lenz & Breger 2005), widely used in astrophysics for multi-frequency analysis of light curves, was employed. The program implements a discrete Fourier transform, which allows for the identification of significant peaks in the amplitude spectrum. These peaks correspond to potential frequencies associated with real periodic variations.

Since photometric observations are not obtained at perfectly regular time intervals, the sampling is irregular. This behavior can introduce artifacts in the frequency spectrum, such as aliases or false peaks. To assess the magnitude of these effects, the spectral window was calculated, which expresses how the sampling pattern responds to different frequencies and can be visualized in **Fig.** 2. Comparing the amplitude spectrum with the spectral window allows for a clearer distinction between which peaks are real and which are an effect of the sampling.

The uncertainties in the parameters of the detected frequencies (frequency, period, amplitude, and phase) were calculated using the Monte Carlo resampling method (Schwarzenberg-Czerny 1991). A total of 1000 synthetic time series were generated by perturbing each original photometric data point $m_i$ within its measurement error $\sigma_i$, assuming a normal distribution. For each synthetic series, the complete Fourier analysis and least-squares fitting were repeated. The standard deviations of the resulting distributions for each parameter were adopted as their $1\sigma$ uncertainties.

Once the most prominent frequencies were identified, the process of fitting sinusoidal models to the observed signal was

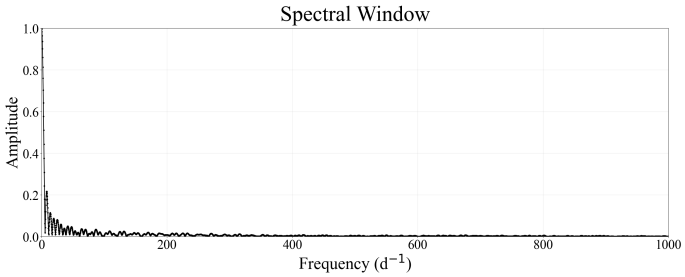


**Fig. 2.** Spectral window of the temporal sampling, which shows the response of the irregular sampling pattern in the frequency domain. The main peaks in the spectral window occur at frequencies corresponding to the reciprocal of the total observation interval (~4.32 hours) and to harmonics associated with the observation gaps.

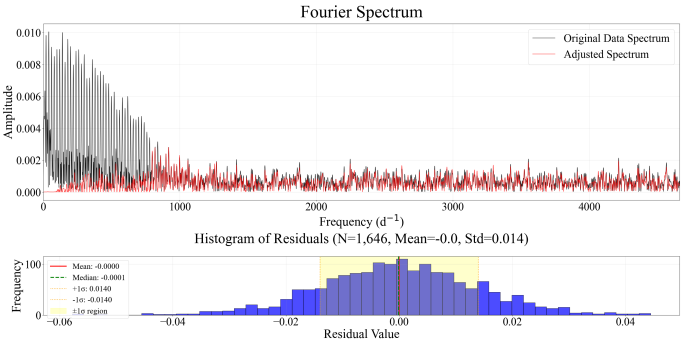


**Fig. 3.** Fourier amplitude spectrum of the photometric time series and histogram of the residual distribution after pre-whitening all detected frequencies.

carried out. Each detected frequency is modeled as a sinusoidal function with a determined amplitude, phase, and frequency. In this way, the light curve can be represented as the sum of several individual oscillations. Subsequently, the residuals of the fit were analyzed, i.e., the difference between the observed data and the model constructed from the detected frequencies. Analyzing these residuals allows for the evaluation of the fit quality and the detection of any additional signals not initially considered. If new periodicities are found, the process is repeated: new frequencies are added to the model, and the residual signal is re-evaluated.

Overall, this iterative procedure allows for refining the detected frequencies, evaluating their significance, and constructing a model that adequately describes the intrinsic variability of the studied stellar system.

## 3. Results and Analysis

The Fourier analysis of the photometric time series revealed two statistically significant independent frequencies, accompanied by multiple harmonics and linear combinations. Sixty-five spectral components were identified and incorporated into the final model. The two fundamental frequencies, along with their corresponding periods, amplitudes, phases, noise levels, and signal-to-noise ratios (S/N), are presented in **Table** 1.

| $f$ [d$^{-1}$] | $P$ [days] | Amp [mag] |
|---|---|---|
| 5.8346±6.08×10$^{-3}$ | 0.1713±1.78×10$^{-4}$ | 0.1909±2.81×10$^{-3}$ |
| 19.7266±5.59×10$^{-4}$ | 0.0506 ±10$^{-5}$ | 1.4589±2.89×10$^{-3}$ |
| $\phi$ [rad] | Noise ×10$^{-}$3 | S/N |
| 0.8113±4.0×10$^{-3}$ | 1.0202 | 40.1395 |
| 0.3464 ±4.0×10$^{-4}$ | 2.6866 | 30.8031 |

**Table 1.** Independent frequencies detected via Fourier analysis. The high signal-to-noise ratio (S/N≫ 4) confirms their statistical significance.

The signal-to-noise ratios exceed the empirical detection threshold of S/N ≥ 4, providing strong evidence for the astrophysical origin of these oscillations rather than instrumental artifacts or aliasing effects.
On the other hand, **Fig.** 3 shows the Fourier spectrum of the original data alongside the spectrum after pre-whitening the detected frequencies. The residual spectrum does not show significant peaks above the noise level, confirming that our model has adequately captured all periodic signals. The residuals follow a Gaussian distribution with a standard deviation of 0.014 magnitudes, which is consistent with the photometric uncertainties.

The detected frequencies and their harmonics were used to construct a multi-frequency model of the following form:

$$m(t) = m_0 + \sum_{i=1}^{2} \sum_{k=1}^{n_i} A_{ik} \sin(2\pi k f_i t + \phi_{ik}) \quad (1)$$

Where $m(t)$ represents the magnitude at a time $t$, $m_0$ is the mean magnitude, $f_i$ are the fundamental frequencies, $A_{ik}$ and $\phi_{ik}$ are the amplitudes and phases for each harmonic, and $n_i$ denotes the number of harmonics for each fundamental frequency.

The multi-frequency model provides an excellent fit to the observational data, as shown in **Fig.** 4. The phase-folded light curves with both fundamental periods reveal coherent pulsation patterns, and the residuals are displayed in the bottom panel, showing no systematic trends and being randomly distributed around zero with a root mean square (RMS) scatter of 0.014 magnitudes.

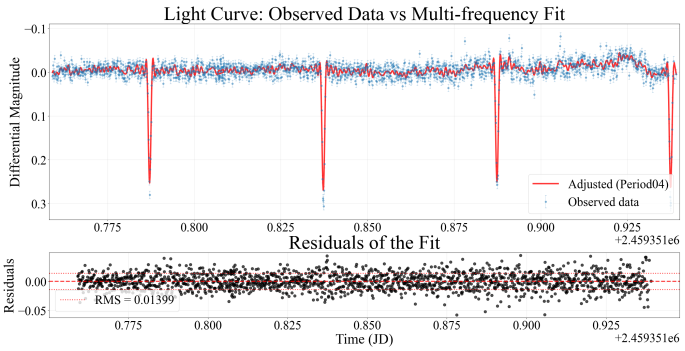


**Fig. 4.** Results of the light curve modeling. Top panel: Observed photometric data with respective measurement error (blue points) with the multi-frequency model overlaid (red line). Bottom panel: Residuals of the fit, showing random scatter with $\sigma$ = 0.014 magnitudes and no systematic trends, indicating a suitable model.

The multi-frequency model, constructed from the two fundamental frequencies ($f_1$ = 5.8346 d$^{-1}$, $f_2$ = 19.7266 d$^{-1}$) and their respective harmonics, reproduces the observed light curve exceptionally well. The overlay of the model with the photometric data shows a high quantitative agreement, confirmed by an RMS residual of only 0.014 mag, a value consistent with the mean photometric uncertainty (~ 7.9 × 10$^{-3}$ mag).

The complex oscillatory structure of the light curve, which combines a long-period modulation ($P_1 \approx 0.1713$ d) with another of shorter period and higher amplitude ($P_2 \approx 0.0506$ d), is fully captured by the model.

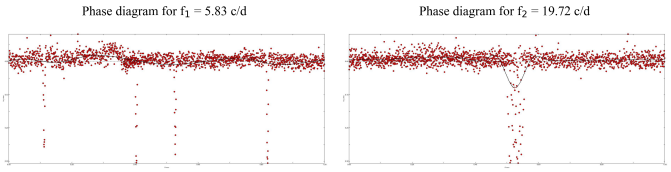


**Fig. 5.** Light curve folded in phase with the frequency $f_1 = 5.83$ c/d, showing a sinusoidal modulation of amplitude $\approx 0.19$ mag. On the other side is the light curve folded with $f_2 = 19.72$ c/d, where a faster and higher amplitude periodic variation ($\approx 1.46$ mag) is observed.

In **Fig.** 5 the phase diagrams corresponding to the two detected fundamental frequencies are presented. For $f_1 = 5.83$ c/d, a clear and coherent sinusoidal modulation is observed, with a photometric amplitude of approximately 0.19 mag. In the case of $f_2 = 19.72$ c/d, the light curve shows a faster and higher amplitude periodic variation (≈1.46 mag). The phase has been folded using the periods derived from the Fourier analysis ($P_1 = 0.1713$ d, $P_2 = 0.0506$ d), confirming the stability of the oscillations throughout the observed interval.

The morphology of the phase-folded light curves reveals distinctive features for each frequency. The $f_1$ signal exhibits an almost symmetric sinusoidal shape, typical of radial pulsations or low-amplitude modulations in binary systems. On the other hand, the $f_2$ curve shows a more complex profile, with possible asymmetries that could indicate tidal elongation effects, stellar spots, or non-radial pulsations.

### *3.1. System Classification*

Based on the detected fundamental frequencies presented in **Table** 1 and the morphology of the phase-folded light curves, it is possible to propose plausible astrophysical scenarios for the studied system. However, due to the short time interval covered by the observations (~4.32 h, equivalent to ~3.5 cycles of the shortest period), the following interpretations should be considered preliminary and subject to confirmation by additional observations.

The dominant frequency $f_2 = 19.7266\,\mathrm{d}^{-1}$, corresponding to a period $P_2 = 0.0506$ d (~1.21 h), exhibits the highest photometric amplitude and a rich harmonic structure. These characteristics, along with the non-purely sinusoidal shape of the folded light curve, are indicative of a periodic geometric phenomenon rather than a simple pulsational oscillation. In this context, $P_2$ is naturally interpreted as the orbital period of the system.

The extremely short value of $P_2$ places the object in the regime of ultra-compact binaries, robustly excluding W UMa-type contact binary systems, whose observed minimum periods are $\gtrsim 0.21$ d (Rucinski 2007; Nelson et al. 2022). Similarly, an sdB+M dwarf system is geometrically unfeasible for this period, given the typical size of a dM-type star.

#### Astrophysically viable scenarios

Las dos frecuencias fundamentales detectadas, junto con su amplia estructura de armónicos y combinaciones lineales, son consistentes con los siguientes escenarios astrofísicos: The two detected fundamental frequencies, along with their extensive structure of harmonics and linear combinations, are consistent with the following astrophysical scenarios:

- HW Vir-type binary with a substellar companion (sdB + BD/WD)
  The period of ~ 1.21 h is characteristic of post-CE systems with hot subdwarfs accompanied by compact objects:
  - For a brown dwarf (BD) companion: Typical periods 0.05–0.15 d, like CD-30°11223 ($P \approx 0.048$ d) Geier et al. (2019); Schaffenroth et al. (2019).
  - For a white dwarf (WD) companion: Periods 0.04–0.20 d, like SDSS J0820+0008 ($P = 0.096$ d).
  - The high amplitude of $f_2$ ($\approx 1.46$ mag) is compatible with deep eclipses of the sdB component by its compact companion.
  - The ratio $P_1/P_2 \approx 3.38$ could correspond to a third body in a hierarchical system or to low-frequency pulsations of the sdB star.
- Cataclysmic Variable (CV) at the minimum period limit
  The period $P_2 \approx 0.0506$ d lies at the extreme lower limit for cataclysmic variables:
  - WZ Sge type: Typical range 0.055–0.080 d, with $P_2$ slightly below the usual minimum.
  - AM CVn type (He donors): Range 0.01–0.05 d, $P_2$ at the upper extreme.
  - Problem: The ratio $P_1/P_2 \approx 3.38$ is incompatible with typical superhumps ($P_{\rm sh}/P_{\rm orb} \approx 1.03$–$1.08$).
  - If $f_2$ is the orbital period, $f_1$ could not be a standard superhump.
- Double degenerate binary (WD+WD)
  Systems with two white dwarfs can reach extremely short periods:
  - Typical range: 0.005–0.1 d Kilic et al. (2021).
  - Example: SDSS J065133.33+284423.3 ($P = 0.0085$ d).
  - Advantage: Naturally explains the ultra-short period and possible deep eclipses.
  - Challenge: Requires near-perfect orbital alignment for eclipses.

#### Interpretations for $f_1$ ($P_1 = 0.1713$ d)

Given the ratio $P_1/P_2 \approx 3.38$, the possible interpretations for $f_1$ are:

- **Hierarchical triple system:**
  - Ultra-compact inner binary ($P_2$) + outer third body ($P_1$).
  - Period ratio of 3.38 is dynamically stable.
  - Would predict eclipse timing variations with period $P_1$.
- **Pulsations of the primary component:**
  - For sdB: low-frequency g-modes (periods up to ~ 0.2 d).
  - For WD: ZZ Ceti-type pulsations (typical periods 0.1–0.3 d).
  - $P_1 = 0.1713$ d is at the upper range for sdB pulsations.
- **Rotational modulation or starspots:**
  - Synchronized rotation of one of the components.
  - Stellar spots on the low-mass companion.
- **Sampling artifact or combination:**
  - Spurious frequency from non-linear combination of other signals.

– Less likely given its high SNR and presence of harmonics.

In **Fig.** 6, the different scenarios can be seen more clearly in a comparative table with probable systems:

| Scenario | Period compatibility | Plausibility | Key evidence |
|---|---|---|---|
| **sdB + Brown Dwarf (BD)** | Good (0.05–0.15 d) | Medium | CD-30°11223 ($P \approx 0.048$ d); requires BD companion |
| **sdB + White Dwarf (WD)** | Excellent (0.04–0.20 d) | High | Naturally explains short period; WD fits easily in orbit |
| **Double Degenerate (WD+WD)** | Excellent (0.005–0.1 d) | High | Shortest periods possible; strong gravitational wave source |
| **CV: AM CVn type** | Marginal (0.01–0.05 d) | Low | $P_2$ at upper edge of range; requires He donor |
| **CV: Extreme WZ Sge** | Poor (0.055–0.08 d) | Very low | Below period minimum; unusual configuration |
| **Compact Triple System** | Excellent | High | Naturally explains $P_1/P_2 \approx 3.38$ ratio |

**Fig. 6.** Evaluation of astrophysical scenarios compatible with $P_2 = 0.0506$ d (1.21 h). The period ranges are based on observational catalogs: sdB+BD (Schaffenroth et al. 2019), sdB+WD (Geier et al. 2019), WD+WD (Kilic et al. 2021), CVs (Ritter & Kolb 2003).

To determine the nature of the detected binary system, a comparative analysis was performed using a period-amplitude diagram. In **Fig.** 7, the observed parameters of the system (red and orange points) are superimposed on the probability regions established for different post-common-envelope astrophysical scenarios. The data show that the main orbital period of 0.0506 days (1.21 hours) and the amplitude of 1.46 magnitudes primarily coincide with the regions corresponding to sdB+WD and sdB+BD systems. The proximity of the point to the minimum period limit (∼0.055 days) suggests an ultra-compact system near the expected minimum orbital period for post-common-envelope binaries.
This systematic comparison allows for ruling out less probable scenarios and establishing the most plausible configurations for the observed system.
On the other hand, the position of $f_1$ (secondary signal) outside the main regions suggests a different origin, possibly related to pulsations of the primary component or the presence of a third body in the system.

## 4. Conclusion

In this work, a detailed multi-frequency analysis of a photometric light curve composed of 1646 observations was carried out using Fourier transform techniques and iterative sinusoidal modeling. The study allowed for the identification of two statistically significant fundamental frequencies with high signal-to-noise ratios, as well as a rich structure of harmonics and linear combinations, evidencing complex intrinsic variability of astrophysical origin.

The dominant signal corresponds to a period $P_2 = 0.0506 \pm 10^{-5}$ d (1.21 h), accompanied by a high photometric amplitude ($A_2 \simeq 1.46$ mag), which unambiguously places the system in the ultra-compact binary regime. The systematic comparison in the period–amplitude diagram rules out scenarios of W UMa-type contact binaries and strongly favors a post–common-envelope configuration, near the observational lower limit of orbital periods for this type of system.

The most plausible scenarios correspond to compact systems such as an sdB+brown dwarf binary, sdB+low-mass white dwarf binary, or alternatively a double degenerate binary (WD+WD). The high amplitude and the morphology of the

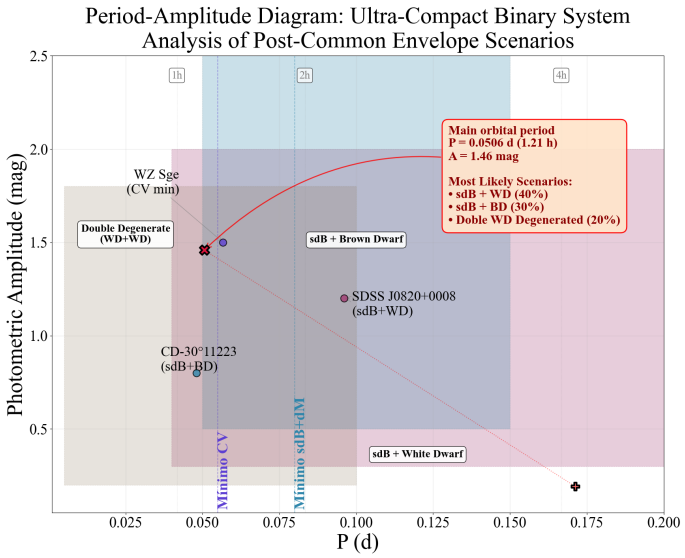


**Fig. 7.** Period-amplitude diagram for the analysis of post-common-envelope astrophysical scenarios. The red ($f_2$) and orange ($f_1$) points represent the observed parameters of the system. The shaded regions correspond to systems: sdB+white dwarf (pink), sdB+brown dwarf (blue), and double degenerate WD+WD (amber). The gray points show reference systems: WZ Sge (minimum period cataclysmic variable), CD-30°11223 (sdB+BD), and SDSS J0820+0008 (sdB+WD). The vertical dotted lines indicate theoretical minimum orbital periods. The period ranges are based on observational catalogs: sdB+BD (Schaffenroth et al. 2019), sdB+WD (Geier et al. 2019), WD+WD (Kilic et al. 2021), CVs (Ritter & Kolb 2003).

light curve are compatible with the presence of deep eclipses or intense reflection effects, characteristic of highly compact post–CE systems.
The detected secondary frequency, associated with a period $P_1 = 0.1713$ d, presents a ratio $P_1/P_2 \approx 3.38$, suggesting an origin distinct from the main orbital period. Among the viable interpretations are low-frequency pulsations of the primary component ($g$ modes in hot subdwarfs or ZZ Ceti-type pulsations in white dwarfs), as well as the possible presence of a third body in a stable hierarchical configuration. The high statistical significance of this signal makes it unlikely to be an instrumental or sampling artifact.

Overall, the results indicate that the studied system belongs to the class of post–common-envelope ultra-compact binaries, constituting a particularly interesting candidate for studies of extreme binary evolution. High-resolution spectroscopic observations will allow for discrimination between the proposed scenarios by detecting characteristic spectral lines of hot subdwarfs or white dwarfs, measuring radial velocities, and searching for signatures of accretion.

## References


Nelson, R. H., et al. 2022, AJ, 164, 115, *The ASAS-SN Catalog of Variable Stars XII*
Rucinski, S. M. 2007, MNRAS, 382, 393, *Contact binaries of the Galactic disk*
Breger, M., Pamyatnykh, A. A., Poretti, E., et al. 1999, A&A, 349, 225
Charpinet, S., Fontaine, G., Brassard, P., et al. 2011, A&A, 530, A3
Frescura, F. A. M., Engelbrecht, C. A., & Frank, B. S. 2013, MNRAS, 429, 191
Geier, S. 2013, Astron. Nachr., 334, 471
Geier, S., Raddi, R., Gentile Fusillo, N. P., et al. 2019, A&A, 621, A38
Heber, U. 2009, ARA&A, 47, 211
Horne, J. H., & Baliunas, S. L. 1986, ApJ, 302, 757
Kepler, S. O., Pelisoli, I., Koester, D., et al. 2015, MNRAS, 446, 4078

Kilic, M., Kosakowski, A., Moss, A. G., et al. 2021, MNRAS, 502, 4976
Kilkenny, D. 2011, Astrophys. Space Sci., 336, 165
Lenz, P., & Breger, M. 2005, Commun. Asteroseismol., 146, 53
Mukadam, A. S., Winget, D. E., von Hippel, T., et al. 2004, ApJ, 607, 982
Percy, J. R. 2007, *Understanding Variable Stars*, Cambridge Univ. Press
Prša, A., & Zwitter, T. 2005, ApJ, 628, 426
Ritter, H., & Kolb, U. 2003, A&A, 404, 301
Samus, N. N., Durlevich, O. V., et al. 2017, Astron. Rep., 61, 80
Schaffenroth, V., Barlow, B. N., Geier, S., et al. 2019, A&A, 630, A80
Szkody, P., Anderson, S. F., Brooks, K., et al. 2011, AJ, 142, 181
Warner, B. 1995, *Cataclysmic Variable Stars*, Cambridge Univ. Press
Schwarzenberg-Czerny, A. 1991, MNRAS, 253, 198